ACS APPLIED MATERIALS & INTERFACES

Biological and Medical Applications of Materials and Interfaces

Mechanical Property of Hydrogel and the Presence of Adipose Stem Cells in Tumor Stroma Affect Spheroid Formation in 3D Osteosarcoma Model

Banani Kundu, A. R. Bastos, V. Brancato, Mariana T. Cerqueira, Joaquim M. Oliveira, Vitor M. Correlo, Rui L. Reis, and S. C. Kundu

ACS Appl. Mater. Interfaces, **Just Accepted Manuscript** • Publication Date (Web): 03 Apr 2019

Just Accepted

ACS Publications

is published by the American Chemical Society. 1155 Sixteenth Street N.W., Washington, DC 20036

Mechanical Property of Hydrogel and the Presence of Adipose Stem Cells in Tumor Stroma Affect Spheroid Formation in 3D Osteosarcoma Model

B. Kundu[1,2], A. R. F. Bastos[1,2,3], V. Brancato[1,2], M. T. Cerqueira[1,2], J. M. Oliveira[1,2,3], V. M. Correlo[1,2,3], R. L. Reis[1,2,3], S. C. Kundu[1,2]

[1]I3Bs - Research Institute on Biomaterials, Biodegradables and Biomimetics, University of Minho, Headquarters of the European Institute of Excellence on Tissue Engineering and Regenerative Medicine, AvePark, Zona Industrial da Gandra, 4805-017 Barco, Guimarães - Portugal

[2]ICVS/3B's - PT Government Associate Laboratory, Braga/Guimarães, Portugal

[3]The Discoveries Centre for Regenerative and Precision Medicine, Headquarters at University of Minho, Avepark, 4805-017 Barco, Guimarães, Portugal.

Corresponding author(s)

B. Kundu (bkundu@i3bs.uminho.pt)

S. C. Kundu (kundu@i3bs.uminho.pt)

Keywords:

Osteosarcoma, Adipose derived stem cells, Cancer microenvironment, Hydrogel, Tissue Engineering

Abstract

Osteosarcoma is one of the most common metastatic bone cancers, results in significant morbidity and mortality. Unfolding of effectual therapeutic strategies against osteosarcoma is impeded due to the absence of adequate animal models, which can truly recapitulate disease biology of humans. Tissue engineering provides an opportunity to develop physiologically relevent, reproducible, tunable *in vitro* platforms to investigate the interactions of osteosarcoma cells with its microenvironment. Adipose derived stem cells (ASCs) are detected adjacent to osteosarcoma masses; considered to have protumor effects. Hence, the present study focuses on investigating the role of reactive ASCs in formation of spheroids of osteosarcoma cells (Saos 2) within a three-dimensional (3D) niche, which is created using gellan gum – silk fibroin. By modifying the blending ratio of gellan gum - silk, the optimum stiffness of the resultant hydrogels such as GG and GG75: S25 is obtained for cancer spheroid formation. This work indicates that the co-existence of cancer and stem cells can able to form spheroid, the hallmark of cancer, only in a particular micro-environment stiffness. The incorporation of fibrillar silk fibroin within the hydrophilic network of gellan gum in GG75: S25 spongy-like hydrogels closely mimics the stiffness of commercially established cancer biomaterials (e.g. Matrigel, HyStem). The GG75: S25 hydrogel maintains the metabolically active construct for longer time with elevated expression of OPN, OCN, RUNX 2 and BSP genes, the biomarkers of osteosarcoma, compared to GG. The GG75: S25 construct also exhibits intense alkaline phosphatase expression in immunohistochemistry compared to GG, indicating the potentiality of it to serve as biomimetic niche to model osteosarcoma. Taken together, the gellan gum – silk fibroin blended spongy-like hydrogel is envisioned as an alternative low-cost platform for 3D cancer modelling.

1. Introduction

Osteosarcoma is the most common and devastating bone cancer in children and adolescents, accounting approximately 20% clinically detectable metastasis at presentation.[1] The ever-rising evidences are indicative of establishment of an autocrine network by cancer cells that remodel tumor microenvironment to fuel disease progression and metastasis.[2-3] Adipose tissue is increasingly considered as the largest endocrine organ in body[3] that recruits adipose-derived stem cells (ASCs) or cancer-related adipocytes into tumor microenvironment, facilitating protumor effects.[4-5] ASCs stimulate the proliferation and metastasis of ovarian cancer cells and are the major component of pre-metastasis niche in omentum.[6] ASCs are also abundant in intermuscular tissue, adjacent to osteosarcoma masses.[7] Further, late local recurrence of osteosarcoma is reported after autologous fat grafts,[8] indicating detrimental role of ASCs in osteosarcoma. Therefore, the present investigation dissects the contribution of ASCs in osteosarcoma invasion and vice-versa in three-dimensional (3D) tumor microenvironment.

The popular strategy to compensate much complex xenografts and inter-species negative barriers on relevance of xenografts[9] is development of 3D *in vitro* tissue models employing tissue engineering strategies. Diverse extra cellular matrix (ECM) resembling natural (such as collagen type I, silk fibroin, fibronectin, hyaluronan etc.) and synthetic materials (e.g. polyethylene glycol, poly-ε-caprolactone and poly-lactic-co-glycolic acid) used in tumor microenvironment engineering, are well elaborated in recent reviews.[10-11] To our best knowledge, none of them addresses the use of protein-polysaccharide composites to recapitulate the physical cues of cancer microenvironment (except few investigations on immobilized hyaluronic acid in gelatin).[12] Generally, ECM biopolymers are categorized into fibrous proteins and polysaccharides; therefore, taking into consideration to include both protein-polysaccharide into ECM modeling of *Cancer* is more appropriate for a clinically relevant model.

The first account of choice for designing tumor microenvironment is a well interconnected 3D stable scaffolding network. The most obvious and extensively used cancer associated extra-cellular matrix scaffold component is collagen, due to its profound complex role in cancer progression, which is identified as tumor-associated collagen signatures.[13] In addition, the hierarchical

arrangement of collagen type I provides the framework to natural bone cells for hydroxyapatite mineralization.[14] Therefore, for culturing human osteosarcoma cells (Saos 2), collagen is the ideal choice as scaffolding material. The commercially available collagen (i.e. type I of bovine origin), which is exploited extensively in research purposes, possesses transmissibility of infectious pathogens due to its veterinary origin[15] with low structural stability for long term culture. Alike col I, silk protein fibroin of Lepidopteran origin is fibrous in nature; supporting long-term co-culture microenvironment of bone and cancer cells including multiple myeloma, breast and prostate.[16]

In this study, we foresee the incorporation of silk protein within the cell-adhesive hydrogel network of Gellan gum, the bacterial exopolysaccharide resembling ECM glycosaminoglycan, is of great utility to regenerate biologically competent bone-like niche. Our strategy for this model is to recapitulate conditions encountered by metastasized osteosarcomas, featuring dynamic mechano-transduction of ECM and cell-cell interaction. During metastasis, the cancer cells remodel the ECM, results in change in pore sizes, porosity, interconnectivity and stiffness.[17] In order to recreate this, we set out to generate a library of gellan gum- silk biomaterials with variable blending ratios to reflect composition induced cellular interaction and tumor spheroid formation. The invasion affinity is analyzed microscopically and revealed by migration of ASCs towards Saos 2 and vice versa. Therefore, tissue engineering approaches not only be able to recreate the damage tissue but also be capable to galvanize cancer research. Data obtained from the present investigation attributes to the insights of cellular cross-talk in relation to cell-cell and cell-matrix communication within osteosarcoma microenvironment, revealing greater caution in using autologous ASCs for cancer and regenerative therapies[18-19] post-chemotherapeutic treatments.

2. Methods and materials

2.1. Preparation of gellan gum-silk spongy-like hydrogel

Aqueous silk fibroin of *Bombyx mori* was prepared as described elsewhere.[20-21] Briefly, removal of silk protein sericin was taken place by boiling silk cocoon cut pieces in sodium carbonate solution (0.02 M, Sigma-Aldrich, St. Louis, MO) for 60 min. The degummed fibers were then rinsed thrice in deionized water, dried overnight and solubilized in freshly prepared aqueous

lithium bromide (9.3 M, Sigma-Aldrich, St. Louis, MO). Silk solution thus obtained was dialyzed against deionized water using cellulose dialysis tubing (Dialysis Tubing, benzoylated, Sigma, USA) over 3 days. After dialysis, aqueous silk solution was centrifuged (at 8000 rpm, 5 ^{o}C, 20 min) to remove the insoluble debris (if any). The concentration of silk solution (S) was determined gravimetrically and adjusted to 2 wt% for hydrogel preparation.

Aqueous solution of gellan gum (GG) was prepared following a standard protocol[22] by dissolving appropriate amount of gelzan powder (2 wt%) (Sigma, USA) in deionized water under constant stirring at 90 °C.

For the preparation of gellan gum (GG)-silk fibroin (S) hydrogels, once the clear solution of gellan gum was obtained, the solution was then cooled down to 45°C for 5 min while stirring vigorously. Silk solution (2 wt%) was added to gellan gum in a ratio of 1:3, 1:1 and 3:1 and represented as GG75:S25, GG50:S50 and GG25:S75 respectively throughout the manuscript [Scheme 1]. The reaction mixture was then mixed gently and casted into molds immediately after adding the cross-linker ($CaCl_2$,10 mM) (Merck Millipore, Germany). Only cross-linked gellan gum hydrogel (2 wt%) was also fabricated and represented as GG.

The hydrogels thus formed were stabilized in PBS solution (pH 7.4, Sigma, USA) for 48 h with successive change in buffer, punched into 8 mm diameter using a biopsy puncher and frozen at -20 °C for 24 h. Spongy-like hydrogels were collected after freeze drying the samples for 3 days using a freeze-dryer (LyoAlfa 10/15, Telstar, Spain).

2.2. Physical characterization of cell free spongy-like hydrogels

2.2.1. Hydrogel topography

To investigate the micro-architecture of the hydrophilic network, the freeze-dried spongy-like hydrogels were sputter coated with platinum (5 nm) and imaged with a JEOL JSM 6301F/Oxford INCA Energy 350/Gatan Alto 2500 microscope. For quantitation, the diameter of 10 randomly chosen pores within an image was measured using ImageJ (National Institutes of Health, version 1.50).[21]

2.2.2. Hydrogel microarchitecture

To further validate the interconnectivity within the spongy-like hydrogels, X-ray microtomography was carried out (μCT1272, SkyScan 1272, Belgium). The samples were scanned dry in air at an energy of 50kV, an intensity of 200 μA and integration time of 1s, with a nominal resolution of ~2 μm. A global threshold of 4.5 % of maximum grayscale value was applied to a dataset of 150 slices to distinct hydrogels from the background and to binarize the images. The resulting 3D volumes were evaluated morphometrically (CT Analyzer v1.17.0.0, SkyScan, Belgium) for hydrogel pore size distribution, porosity and pore wall thickness as described previously.[22] The 3D virtual models of the representative regions were also generated using image processing software (CT-Vox and Dara Viewer, SkyScan, Belgium).

2.2.3. Mechanical stability

Spongy-like hydrogels were equilibrated in PBS at room temperature (~ 24 h), placed in a confined sample holder and the compressive strength was investigated under static compression using an INSTRON 5543 (Instron Int. Ltd., USA) equipped with 10 N load cell. The samples were subjected to a pre-load of 0.1 N, tested up to 85 % of strain at a loading rate of 2 mm min^{-1}.

2.2.4. Contact angle measurement

The wettability of the samples was measured by adding a droplet of deionized water (5 μl) on cylindrical 3D dried sponge surfaces. The contact angle at the intersection of liquid and solid surface was measured using a Goinometer (OCA 15PLUS, DataPhysics, Germany).

2.2.5. Water uptake

Pre-weighed dried sponges were submerged in PBS (pH 7.4) for up to 7 days at 37°C to investigate the water uptake profile of the spongy-like hydrogels. At each pre-determined time interval, excess water from the surface of the hydrogels was wiped out using paper towels and weighed. The water content of hydrogels was determined as follows:

$$\text{Water uptake (\%)} = {}^{(Ww - Wd)}\!/_{Wd} \times 100$$

Where, Wd is the weight of dried state and, Ww is the weight of the wet state of hydrogels

2.2.6. Stability of the hydrogels

The stability of gellan gum-silk fibroin spongy-like hydrogels was assessed as a function of released protein fibroin from the composite constructs over time.[21] Concisely, the hydrogels were incubated within the known volume of phosphate buffer saline (PBS, pH 7.4) containing 0.02 wt.% sodium azide (to avoid fungal contamination) at 37°C, followed by the collection of PBS extracts regularly at pre-selected time intervals.

The amount of protein released in solution was determined using Micro BCA assay at 562 nm using a microplate reader (Microplate Reader - Gen 5 2.0, BioTek, USA). Absorbance readings were translated into protein concentrations using a calibration curve built using known silk fibroin dilutions.

2.2.7. Structural conformation

The infrared spectra of gellan gum-silk hydrogel films were obtained using ATR-FTIR spectrophotometer (IRPrestige 21, Shimadzu, Japan). The samples to be analyzed were placed onto ATR and spectra were obtained in the range of 4000–400 cm^{-1} at an average of 25 scans and resolution of 4 cm^{-1}.

2.3. Cell isolation and culture

Human adipose-derived stem cells (ASCs) were acquired from the Hospital da Prelada (Porto, Portugal) with patient's informed consent after liposuction and processed at 3B's Research Group following the ethical guidelines approved by both the Institutions.[22-23] The ASCs were then characterized by flow cytometry before use. Briefly, ASCs (P2) were resuspended in a 3% BSA (Sigma-Aldrich, France) solution and incubated for 30 minutes at room temperature, following manufacturer-recommended concentrations, with mouse anti-human antibodies CD105-FITC, CD73-PE, CD90-APC, CD45-FITC and CD34-PE (BD Biosciences, Germany). Cells were subsequently washed with phosphate-buffered saline (PBS) (Sigma, USA), centrifuged, fixed in 1% paraformaldehyde (Sigma, USA) and analysed on a FACS Aria III (BD Biosciences, USA) using BD FACS Diva Software version 7.0.

Saos 2 cells were procured from the European Collection of Cell Cultures (ECACC, UK). Both types of cells were maintained in αMEM supplemented with 10% fetal bovine serum (FBS) - 1% penicillin/streptomycin at 37°C and 5% CO_2-humified atmosphere. ASCs till passage 2 were used for the experiments.

2.3.1. Preparation of cell embedded 3D compartmentalized-hydrogel system for co-culture

Freeze-dried spongy-like hydrogels were sterilized with ethylene oxide treatment (EO; 3 h at 52 °C), followed by wetting using dilute alcohols (70% ethanol) under UV light in sterile hood. The sterilized hydrogels were then punched individually into a core (~ 5 mm), which yielded doughnut shaped counterpart (outer ring) (scheme 2). The hydrogels (both inner core and doughnut shaped outer ring) were rinsed several times with sterile PBS (pH 7.4) to remove the traces of alcohol. Each hydrogel was individually transferred into separate culture wells (marking specifically each core with respective to its doughnut counterpart) and hydrated by soaking overnight in αMEM supplemented with 10% fetal bovine serum (FBS) at 37°C and 5% CO_2-humified atmosphere. Prior to cell seeding, the medium was taken out and the hydrogels were left for partial dehydration (~ 4 h).[21,24]

Cells after reaching to 90 % confluence, were trypsinized, centrifuged and brought into suspension using fresh αMEM supplemented with 10% fetal bovine serum (FBS) - 1% penicillin/streptomycin. For co-culture, both cells, Saos 2 (approximately $1x10^5$ cells to per core hydrogel) and ASCs (approximately $5x10^4$ cells to per doughnut shaped hydrogel) seeded dropwise (10 µl αMEM containing desired cell concentration) on the top of partially dehydrated hydrogels, while placed in separate wells of 24 well plates (coated with 1 wt.% agarose). The cell laden constructs were then left undisturbed for 30 min at 37°C and 5% CO_2-humified atmosphere for cellular infiltration. To keep the total cell number same per construct, for monoculture, approximately $1.5x10^5$ cells in 10 µl αMEM for both Saos 2 and ASCs were seeded at the respective part of the compartmentalized hydrogels (while the other part left non-seeded) as described above and left uninterrupted for cellular infiltration. After initial cellular adhesion, adequate amount of media (500 µl in each well of 24 well plate) was then dispensed slowly at the corner of each well using pipette and the cell-laden hydrogels were left overnight separately.

Next, the doughnut shaped hydrogels were placed back into its corresponding core (both homotypic and co-culture system). The resultant 3D compartmentalized-hydrogel systems were then maintained at 37°C and 5% CO_2-humified atmosphere. The medium was replaced in every alternate day.

2.3.2. Proliferation of cells within the compartmentalized-hydrogel constructs

The proliferation of cells within the constructs with respect to time was measured using Alamar blue assay (Alamar Blue, Bio-Rad, England). At each pre-selected time point, the medium was aspirated, the constructs were rinsed gently with PBS and incubated with Alamar blue (10% v/v, diluted in basal culture media) for 4 h at 37 °C - 5% CO_2. The fluorescence of Alamar blue was measured using a spectrofluorometer (Synergy HT, Bio-Tek, USA) at excitation and emission wavelength of 530 and 590 nm, respectively.

The amount of DNA per construct was also quantified at each time point using Picogreen dsDNA assay kit (Alfagene, Portugal). Briefly, at each time point, the media was taken out from each construct. The constructs were then washed gently with sterile PBS and then transferred to 1.5 ml Eppendorf tube containing 1 ml ultra-pure water. The tubes were then placed into water bath at 37 °C for 1 h, followed by - 80 °C for 1 h. The content of each Eppendorf tube was then thawed and briefly ultrasonicate.[25] Cell lysates were then diluted using assay kit buffer prior to quantification. The DNA concentration in constructs was obtained by comparing the values against a standard DNA curve (0.2 to 2 μg/ml) and used to normalize the cell proliferation values.

2.4. Microscopy and image analysis

At the end of the culture, the constructs were rinsed with PBS and fixed in 10% formalin (Enzifarma, Portugal) for 30 min at room temperature. After fixation, the constructs were washed with PBS again.

To envision actin filaments, the cells were stained using rodhamine-labeled phalloidin (1:500 v/v in PBS, Sigma-Aldrich, USA) and counterstained with 4′,6-diamidi- no-2-phenylindole (DAPI, 1:1000 v/v in PBS, Sigma-Aldrich, USA) for nuclei at room temperature. After staining, the constructs were rinsed in PBS and imaged using inverted confocal microscope TCS SP8 (Leica

Microsystems, Germany). The samples were observed by using fluorescence λex = 415 nm and λem= 461 nm for nuclei, and λex = 560 nm and λem = 630 nm for actin filaments.

The morphologies were further investigated using scanning electron microscope after dehydrating the fixed samples in a gradient series of ethanol solutions and dried using critical point dryer (Critical Point Dryer (Autosamdri-815, Series A, Tousimis). The dried samples were then sputter coated with platinum (5 nm) and imaged with a JEOL JSM 6301F/Oxford INCA Energy 350/Gatan Alto 2500 microscope.

2.5. Histology and Immunohistological (IHC) analysis

The fixed constructs (after formalin fixation as mentioned above) were subjected to standard histological tissue processing for paraffin embedding (EC350-2, Microm, Thermo Scientific, Waltham, MA, USA). Sections of 5 μm thickness were obtained using a microtome (HM355S, Microm, Thermo scientific). The sections were stained with hematoxylin-eosin (H&E) (05-12011/L, 05-M10003, Bio-optica) following a standard protocol and using an automatic stainer equipment (HMS740, Microm, Thermo Scientific).

For collagen, the sections were stained with Masson Trichrome (with aniline blue) assay kit (04-010802, Bio-Optica Milano S.p.A.) following manufacture's protocol.

For IHC, mouse IgG monoclonal antibody for Alkaline Phosphatase (ab126820, Abcam, UK, at 1:100 dilution) was used. Detection was done by using Alexa Fluor® 488 donkey anti-mouse IgG (A21202, Invitrogen, CA, at 1: 500 dilution) and counterstained with DAPI.

All sections after staining were dehydrated and mounted with Entellan® (4111, Inopat) before being observed under a transmitted and reflected light microscope (Leica DM750, Germany) with an MRc5 camera.

2.6. 3D time-lapse confocal microscopy

Cells were fluorescently labeled with CellTrackers, ASCs were labelled with PKH26 Red Fluorescent Cell Linker (Sigma-Aldrich, MO, USA), while Saos 2 were labelled with PKH67 Green Fluorescent Cell Linker (Sigma-Aldrich, MO, USA) for easy visualization. Briefly, cells after trypsinization were washed with serum free media and incubated with dye (1x dye prepared

in Diluent C provided in the kit) for 5 min. After incubation, equal volume of fetal bovine serum was added to dye mixture to stop the reaction. Fluorescently labeled cells were then washed twice with complete media to remove the traces of dye. Approximately 5 x 10^4 cells of each type (in 10 µl αMEM) were seeded in the respective compartment of the compartmentalized-hydrogel system as mentioned in Section 2.3.1. The cells were allowed to adhere to the constructs overnight in an ultra-low-attachment six-well plate (coated with 1% agarose for low-attachment).[26] Cell movement was imaged under a confocal microscope TCS SP8 (Leica Microsystems, Germany) at 490 nm (PKH67) and 551 nm (PKH26) excitation and time-lapse series of 7 days interval (Day 1, 7 and 14). Attention was paid to discriminate cell-mediated contraction from cell migration. Cell contraction was marked by buckling of micro-architecture of the constructs compared to surrounding. The overnight incubation time post-seeding and prior to initial confocal imaging was to allow cell contraction to occur. Care was also taken to maintain the sterility of the constructs during imaging and kept back to culture after imaging. The medium was replaced in every alternate day.

2.7. RNA isolation and real-time RT-PCR

Total mRNA was extracted from GG and GG 75: S25 constructs (from the complete compartmentalized hydrogels as the core and doughnut shaped outer part sealed into one) on day 14, using TRI Reagent® RNA Isolation Reagent (ThermoFisher Scientific, Germany), according to the manufacturer's guidelines. The concentration and purity of RNA were measured by mean of Nanodrop® ND-1000 spectrophotometer (ThermoFisher Scientific, Germany). The synthesis of cDNA was carried out using qScriptTM cDNA Synthesis Kit (Quanta BioSciences, USA). Final volume of 20 µL reaction mix was prepared adding nuclease-free water, 4 µL qScript Reaction Mix, 1 µL qScript Reverse Transcriptase (RT) to the mRNA template (100 ng total RNA). The single-strand cDNA synthesis was occurred by incubating the complete reaction mixture for 5 minutes at 22°C, followed by 30 minutes at 42°C and terminated with an incubation of 5 min at 85°C. RT-PCR was performed using PerfeCTA® SYBR Green FastMix (Quanta BioSciences), following manufacturer's instructions, on RT-PCR Mastercycler Realplex machine (Realplex, Eppendorf). Primer sequences (Eurofins Genomics, UK) were designed using Primer-BLAST tool (details are included in Table 1). Livak's method ($2^{-\Delta\Delta Ct}$) was used to quantify the relative gene expression.[27] The mRNA expression was first normalized to the average expression of internal

housekeeping gene (glyceraldehyde-3-phosphate dehydrogenase, *GAPDH*). Three samples of each condition were considered and the results are represented as fold change towards the gene expression in the GG condition.

2.8. Statistical analysis

Results were represented as mean ± standard deviation (SD). Comparisons of data were performed using one-way analysis of variance (ANOVA) followed by Tukey's test. Statistical significance was considered at $p < 0.05$; except for gene expression $p < 0.01$. The experiments were carried out in triplicates (or otherwise mentioned) for standards and references.

3. Results

3.1. Impact of matrix composition on the architecture of spongy-like hydrogels

Ionic cross-linking chemistry was used to chemically cross-link gellan-gum at low temperature (Scheme 1). The reaction was rapid, yielding stable ionic bonds between Ca^{2+} and -COOH groups of gellan-gum. Silk was initially inter-penetrating within the cross-linked network of gellan-gum, yielding the semi-interpenetrating network of protein-polysaccharide ECM-like hydrogel. The porosity and interconnectivity of the spongy-like hydrogels were revealed by scanning electron micrographs (Figure 1(A)). Adding silk fibroin (S) into GG caused the loss of lamellar formation, improving the micro-porous nature, while incorporating fibrillary-like structure into the network (Figure 1(A)). The incorporation of further $-COO^-$ groups from amino acid side chains of silk fibroin within gellan gum network reduced the rapid aggregation of gellan gum double helices. This retarded the immediate formation of ice-crystals, resulting in larger pores as characterized by X-ray μCT (Figure 1(B)). Figure 1(C) shows hydrogel microstructure as a function of composition. GG-hydrogels exhibited wide distribution of pores ranging from 34 – 60 μm (average 42 ± 14 μm) with ~ 92 % porosity, while GG75: S25 revealed relatively narrow distribution of pores, 53 – 70 μm (average 65 ± 13 μm) with ~ 93 % porosity. The GG50: S50 and GG25: S75 hydrogel revealed average pore size of 64 ± 15 μm (with ~ 91 % porosity) and 60 ± 27 μm (with ~ 90 % porosity), respectively. The incorporation of fibroin, improved the interconnectivity of hydrogel (up to GG50:S50) (Figure 1(D)). However, silk as major component of the hydrogel reduced the interconnectivity due to collapsing or highly aggregated network.

3.2. Interpenetration of fibroin manipulates matrix rigidity and wettability

The control over micro-architecture of spongy-like hydrogels via blending ratios of initial polymer mixture further allowed to tune the mechanical cues of the hydrogels very effectively. To ensure the mechanical properties of the fabricated hydrogels, compression mechanical testing was carried out. The compressive modulus of GG-S blended spongy-like hydrogels is represented in Figure 2(A). Among all spongy-like hydrogels, GG25: S75 exhibited the highest average compressive modulus of 2.48 ± 0.8 kPa compared to 0.416 ± 0.2 kPa of GG hydrogels. However, more variation in results were observed in blended spongy like hydrogels compared to pure GG hydrogels. The stiffness of GG75: S25 was 0.575 ± 0.1 kPa. Surface wettability of the hydrogels was investigated by water contact angle. The hydration degree of porous GG-S spongy-like hydrogel ranged from $34^{o} \pm 4^{o}$ to $88^{o} \pm 6^{o}$, while only GG exhibited $28^{o} \pm 1^{o}$ [Figure 2(B)].

3.3. Blended hydrogels (GG-S) represent stable protein interpenetration within GG, but declining water content

All dried spongy-like hydrogels readily uptake water, reached an equilibrium within 48 h independent of composition (Supplementary Figure 1(A)). Not much differences were observed between blends and pure GG (2467 ± 95 after day 7) except GG50: S50 (3720 ± 91 after day 7), which revealed significantly larger amount of water uptake (in %) among all. The GG75: S25 and GG25: S75 revealed swelling ratio (in %) of 1980 ± 117 and 2396 ± 69, respectively after day 7. The penetration of fibroin within the cross-linked gellan gum was stable, approximately 85% of initial protein concentration remain entrapped within the fabricated hydrogels at the end of 14 days [Supplementary Figure 1(B)].

To understand the interaction between protein – carbohydrate within the semi-interpenetrating network, FTIR analysis was carried out [Supplementary Figure 1(C)]. The FTIR spectra of pure silk fibroin[28] and gellan gum[29] have been well described. The characteristic vibrational modes of amide II (1600-1480 cm^{-1}) is attributed to coupling of N-H in-plane bending and C-N stretching mode and amide III (1350-1100 cm^{-1}) is due to C-N stretching coupled to the in-plane N-H bending mode.[28] In addition, the adsorption bands with 1480-1350 cm^{-1} and 1190-700 cm^{-1} regions are attributed to vibration of amino acid side chains and perhaps contributed little to the

intensity of characteristic protein amide bands. Gellan gum exhibited an absorption band at 2960 cm^{-1} due to sp^3 hybridization of C-H stretching of branched alkane and at 912 cm^{-1} due to alkane C-H bending.[29] The spectrum of the blended hydrogels of gellan gum and silk fibroin was no more than an overlapping spectrum of two, confirming the physical entrapment of silk within the cross-linked network of gellan gum.

3.4. Cell culture

In spite of increasing understanding about the influence of stem cells on tumor evolution, the knowledge of their direct effect on cancer cell behavior is still elusive due to the limitation of mimicking the physiological 3D tumor micro-niche. To gain greater insight of cancer spheroid formation, the advantage of compositional and mechanical versatility of fabricated hydrogel library was taken into consideration in this investigation.

3.4.1. ASCs identification

After initial culture and passages, ASCs exhibited the typical fibroblast-type morphology, as observed in Supplementary Figure 2. The investigation of surface markers by flow cytometer confirmed that these cells express the typical panel of markers characteristic of mesenchymal stem cells >90% expression of CD105/73/90 and <2% CD45/34 (Figure 3(A)).[30]

3.4.2. The proliferation of cells within 3D compartmentalized hydrogels

Alamar blue cell proliferation assay was performed with cell-laden compartmentalized hydrogels of diverse compositions (Figure 3(B)). At the beginning, cells co-cultured in GG75: S25 exhibited greater rate of proliferation, compared to other hydrogel compositions. With time, proliferation rate in all co-culture system independent of composition increased. Similar phenomenon was observed in homotypic/mono cultures (Supplementary Figure 3). The Saos 2 cultures revealed higher cell proliferation at day 1 compared to ASCs, followed by relatively comparable cell proliferation at the end of day 14. The content of DNA in co-culture system was quantified as a measure of cell proliferation and corroborated with Alamar blue cell proliferation assay (Figure 3(C)).

3.4.3. Mechanically dynamic hydrogels recapitulate the physiological niche for spheroid formation

With the aim to find out which hydrogel recapitulates the optimal biomimetic property for the formation of cancer spheroids (i.e. sphere-like three-dimensional cellular aggregate), all the fixed constructs (i.e. cell laden hydrogels) were stained with phalloidin (for actin) and counter stained with DAPI for nuclei after 14 days of culture. Cells co-cultured into softer spongy-like hydrogels such as GG and GG75: S25 (0.4 kPa and 0.6 kPa respectively) facilitated the formation of spheroids, which were localized at the core/center part of the co-cultured compartmentalized hydrogels (Figure 3(D)). In contrast, the homotypic cultures in GG and GG75: S25 and co-culture systems on other hydrogels resulted flatten cell morphologies throughout the compartmentalized hydrogels (Figure 3(D)). Phalloidin staining of spheroids indicated irregular cortical actin staining in GG with ellipsoidal-like cellular aggregates. Typical interwoven cortical actin with dense packing of nuclei indicative of well cell-cell interactions in spheroid of GG75: S25 (Figure 3(D)). However, some disintegration of actin filament was also observed (as indicated by white dotted square). ASCs alone revealed filopodia like structures with various length in diverse hydrogels.

Furthermore, visualization of complete field of compartmentalized hydrogel constructs revealed the confinement of spheroids only into the central portion (core) of the spongy-like hydrogels [GG, Figure 4(A) and GG75: S25 Figure 4(B)]. Gene analysis of the corresponding constructs (GG and GG75: S25) further confirmed a slightly upregulation of expression related to the osteosarcoma [Osteopontin (OPN),[31-32] Bone sialoprotein (BSP),[33] Osteocalcin (OCN),[34] and Run related transcription factor 2 (RUNX 2),[35] when the cells (ASCs and Saos 2) were co-cultured on GG75:S25 [Figure 4(C)]. These genes are considered as clinical markers of osteosarcoma and the obtained results revealed a more aggressive phenotype of the cells laden into GG75: S25 compartmentalized hydrogel. Immunohistochemical analysis of Alkaline Phosphatase (ALP) is used to discriminate other primary bone tumors from osteosarcoma and considered to be superior to OCN in osteosarcoma diagnosis.[34] Positive immunoreactivity of ALP was observed in both GG and GG75: S25 constructs, however, more intense in GG75: S25 [Figure 4(D)]. In addition, the stiffness of GG75: S25 hydrogel (0.6 kPa) was closely mimic the stiffness of Matrigel (0.98 ± 0.30 kPa) and HyStem (a hyaluronic acid-based hydrogel) (0.64 ± 0.15 kPa), the commercially

available hydrogels used for cancer spheroid culture.[36] Recognizing this, we focused all further cellular investigations with GG75: S25 compartmentalized co-cultured constructs.

The characteristic phenomenon of multi-cellular spheroid is its 3D morphology, which is confirmed by Z-height (Z-stack) imaging of GG75: S25 constructs (Figure 4(E)). The histological findings (Figure 5(A)) revealed the confinement of spheroids only into the central portion of the gel (core), which well corroborated with confocal images [Figure 4(B)]. Masson's trichrome staining of collagen demonstrated the deposition of newly formed collagen (Figure 5(B)), which sealed the compartmentalized constructs into one as observed in scanning electron micrograph (Figure 5(C)).

3.4.4. Homing of ASCs into engineered osteosarcoma

Fluorescence micrographs (Figure 4(B)) and histological analysis (Figure 5(A)) revealed the colonization of cells into the central core and formation of cell aggregates or spheroids. Thereby, the migration of ASCs (as they were seeded on outer compartment) toward the core was investigated in time dependent manner. For visualization, the ASCs were stained with PKH26 Red Fluorescent Cell Linker. Cells were expected to migrate along the struts of the hydrogel — the phenomenon referred as contact guidance. ASCs exhibited non-straight-line movement through the spongy-like hydrogels.

4. Discussion

The development of pre-clinical model of osteosarcoma is challenging due to the dynamic mechanical robustness of ECM during disease progression, spheroid formation and hypoxic phenomena of solid tumor. The cross-talk of cells with its niche regulates the fate of the cells. To our best knowledge, no exploration of cellular cross-talk of ASCs and Saos 2 in 3D dynamic mechanical environment has been done. Hence, the present study demonstrates the possibility of using silk fibroin and gellan gum blended spongy-like hydrogels as physiological cancerous niche to recapitulate the 3D mechanical dynamic of cancer. Saos 2 cells, obtained from metastatic human tumor, is osteoblastic in nature with unlimited *in vitro* proliferation ability. Thus, one of popular choice to model osteo-carcinoma. The ASCs used in the present study, are obtained from adipose

tissue adjacent to knee. Therefore, inherits multiple aspects of ASCs of skeletal niche and a rational choice.

The phenomenon of semi-interpenetrating network is employed to establish protein-polysaccharide ECM-like hydrogel. After inter-penetration, the -COO^- groups of fibroins interact with Ca^{2+} of $CaCl_2$, further maturing the hydrophilic network.[37] These hydrogels thus formed are stabilized in phosphate buffer saline (PBS, pH 7.4) to attain the equilibrium state by ion-exchange. Ions from high-ionic external aqueous solution entered into the hydrophilic network based on its elasticity and enhanced the formation of self-assembled anti-parallel double-helices of gellan-gum.[38-39] In nature, the concentration of Ca^{2+} (from 5 to 15 mM) and K^+ (from 5 to 8 mM) within the glands of silkworms enhances as silk advances towards spinneret, lowering the pH of silk solutions.[37] At low pH, the repulsion among silk fibroin molecules decreases, resulting in strong inter-chain interactions and sheet structure through hydrophobic interaction leading to sol-gel transition. Hence, the post-fabrication stabilization using PBS, augments the degree of cross-linking of polymeric network.

The pores of 42 to 65 μm are ideal for cellular infiltration and nutrient diffusion. Present investigation demonstrates relative preference of cells towards blended spongy-like hydrogels, perhaps due to the presence of bioactive silk.[20] The study further confirms the models of metabolic coupling, in which ASCs after activated by osteosarcoma, promote the tumor growth [Supplementary Figure 3].[3] In contrast to 2D culture, 3D cancer spheroids are obtained in hydrogel with stiffness of 0.4 – 0.6 kPa, indicating optimum cell-cell and cell-matrix interaction, exerts at certain intermediate ECM stiffness (Figure 2(A)). Our data further contribute to growing literature on regulation of cancer spheroid formation by ECM stiffness.[36] The co-relation between ECM stiffness and cell migration has been first described for vascular smooth muscle cells[40] and herein, we reported similar relation for human adipose stem cells.

Initial cell adhesion takes place by non-receptor mediated interactions between cell surface molecules and substrate groups of surfaces via electrostatic or polar interactions and ionic bonding,[41] which is demonstrated by contact angle of individual surfaces. The diverse values of contact angles in blends is due to the content of hydrophobic silk fibroin within the inter-

penetrating network and micro-porosity of different surfaces. Porous architecture forms air-pockets, which affect the contact angle of water, preventing the spreading of the drop on surface.[42] The greater experimental contact angle, therefore, generates from air-pockets trapped at solid-liquid interphase, which is expected to prolong the cell adhesion time. Swelling kinetics of hydrophilic network is usually explained by means of (i) the rate of infusibility of solvent and (ii) rate of relaxation of polymeric network.[43] High cross-linking of gellan gum (GG and GG75:S25) and silk fibroin (GG25:S75) in spongy-like hydrogels restricts the swelling behavior. This is well corroborated with the interconnectivity of the hydrogels (Figure 1(A)). The initial release of protein immediately after half an hour post-casting is due to the unreacted free protein, collected in PBS.[21] Thereafter, quantitatively negligible release of protein is obtained, indicative of stable blended network.

Non-immune mesenchymal cells, like fibroblasts and their precursor mesenchymal stem cells are the determinant player of cancer niche, where they are "trained" by neoplastic cells and vice-versa.[5,44] An augmented level of ASCs migration into osteosarcoma and stimulated disease progression have been observed upon co-culturing ASCs with Saos 2 in conventional plastic-adherent conditions.[3] In the present study, a qualitative analysis of ASCs-Saos 2 in 3D co-culture system has been carried out, which concludes beyond doubt that ASCs facilitate osteosarcoma tumor formation in 3D micro-niche. The simplest conventional model of ASCs— Saos 2 co-culture is mixed the cell populations,[45] in which the two cell-types are in direct contact with each other that restricts the systematic investigation of migration of sub-population of cells. Porous membrane, a popular approach, is used to compartmentalize the co-culture of endothelial cells and astrocytes to study the blood-brain barrier but fails to establish effective contacts between cell types due to the nature of porous membrane.[46] Therefore, a compartmentalized culture model is developed that offers the spatio-temporally regulated microenvironment to incorporate effective cell-cell contacts, while allow easy monitoring and facile scale-up with high-throughput systems.

It is well documented that cancer cells induce increasing number of stem cells during initial encounter, which later be beneficial for tumor progression due to the capillary producing capabilities of ASCs.[47] The rate of cell proliferation in 3D co-culture condition in present study also corroborates well with conventional plastic-adherent culture system, which reveals a decrease

in mean doubling time of ASCs-Saos 2 (36 h) compared to ASCs alone (72 h) as reported by Paino et al.[45] Conversely, the findings of Wang et al.,[3] suggest that ASCs promote the proliferation and metastasis of osteosarcoma (Saos 2) by activating signal transducer and activator of transcription 3 (STAT 3). Together, the rate of cell proliferation is more in co-culture condition compared to homotypic culture system, which is observed at the end of the present study (at day 14) (Supplementary Figure 3). Notably, GG75: S25 reveals the highest rate of proliferation in ASCs - Saos 2 system throughout the culture time (Figure 3(C)) suggesting the larger-interconnected pores facilitate cell infiltration/migration.[22] The discrepancy exhibited in terms of over-estimation of cell proliferation by metabolic assay in comparison to Picogreen dsDNA assay (DNA binding fluorophores) is due to mis-correlation of metabolic activity of cells with cell density, which exhibits a non-linear function especially in case of high cell density (such as cancer cells) or while assessing cell proliferation in 3D matrix.[48] The decreasing intensity of fluorescence of cell tracker dye is consistently been corelated with cell proliferation and well corroborated with the fluorescent membrane intercalating dye PKH 26.[49] In contrast, an disagreement is reported in dye transfer behavior of green fluorescence probe PKH67, reveals an increased fluorescence intensity in the apoptotic or transitional cells (apoptotic and necrotic cells), while decreased fluorescence in necrotic cells.[50] The increased intensity at later stage of the culture is unlikely due to released dye from necrotic cells perhaps reuptake by other viable cells, results in increased intensity.[50] The lack of tumor spheroid formation and dwindling rate of proliferation in certain 3D conditions are the reflection of inability of substrate composition to mechanically transduce physiological cancer micro-niche.

As the mechanics and architecture of ECM varies widely, the morphology and migration of cells attune to these biophysical variations.[5149] Given the versatile biophysical characteristics of ECM *in vivo*, it is challenging to design dynamic ECM-cell models that unwind the systematic deconstruction of how the cells respond to these inputs. Our data demonstrate that by integrating the approaches of tissue engineering and biomaterial designing, a myriad signal producing 3D cancer niche can be developed, which undergoes change in substrate alignment on command. The on-command change (by manipulating the blending ratio of polymers) in substrate pore size, stiffness and fibrillar versus non-fibrillar architecture effectively influence cell morphology at cancerous niche.

Besides the application in cancer therapy or diagnostic of early marker, the investigation of stem cell motility through mechanically dynamic 3D hydrogels improve extensively the knowledge of stem cell base therapies with the aim of site specific-delivery of stem cells for tissue repair. The 3D compartmentalized culture system developed herein, can further be used not only for screening of chemotherapeutics but also to direct stem cell as delivery vehicles of chemical cues. However, the investigation of guided cell migration in absence of any growth factors and only by scaffold architecture, is still elusive. The culture system used in the present study is compatible with most standard microscopy techniques that eventually play role in high-throughput screening.

Limitations inherit in the present investigation includes the recognition of chemokines (secreted by osteosarcoma cells) that governing the migration of stem cells towards cancerous niche, providing further opportunity of detection of early stage metastatic markers. Moreover, the detail study of recruitment mechanism of ASCs in bone tumor formation needs to be addressed. Also, the stemness of the construct after co-culture is needed to be investigated in order to get the insight of cancer stem cells. Only qualitative analysis of cell spheroids is considered in the present study. The critical regulator of cancer stroma, the MMPs mediated cross-talk between cellular and non-cellular components may provide precise information on matrix re-modeling and construct stemness — is the scope of future study.

5. Conclusion

The gellan gum-silk fibroin spongy-like hydrogels designed herein results versatile nano-micro architectures and mechanical stiffness, which can be regulated simply by blending ratios of polymers. The GG75: S25 spongy-like hydrogel with the compressive modulus of ~ 0.6 kPa, exhibits a favorable tissue mimetic micro-niche for co-culturing human osteosarcoma and adipose derived stem cells that resembles the *in vivo* solid tumor like morphology of osteosarcoma. Co-cultured Saos 2- ASCs also reveals elevated expression of osteosarcoma biomarkers including osteopontin, bone sialoprotein, osteocalcin and Run related transcription factor 2. The therapeutic implications of the co-culture system are notably, from identification of unique cancer phenotype associated with Saos 2-ASCs cross-talk that can serve as early marker of disease progression — to the establishment of practicalize 3D co-culture system that opens new avenue in tumor-

repopulating cancer cells identification. The system also well paired with conventional microscopy techniques, therefore, may serve as high-throughput screening platform. The simplicity in fabrication process and mechanical versatility of the resultant hydrogel system, anticipate it as an attractive choice to elucidate the critical role of biophysical cues such matrix stiffness to regulate polarized cell motility and tumor formation.

SUPPORTING INFORMATION

Swelling ratio (%), cumulative protein release, FT-IR, time and composition-dependent proliferation of cells under homotypic and heterotypic conditions results. The morphology of ASCs in monolayer.

Acknowledgements

This work is supported by the European Union Framework Programme for Research and Innovation Horizon 2020 under grant agreement nº 668983 — FoReCaST, and FROnTHERA (NORTE-01-0145-FEDER-000023). VM Correlo acknowledges Investigator FCT program (IF/01214/2014), MT Cerqueira acknowledges NORTE-01-0145-FEDER-000021 and JM Oliveira to the program Investigator FCT2015 (IF/01285/2015).

References

(1) Anderson, M. E. Update on Survival in Osteosarcoma. *Orthop. Clin. North Am.* **2016**, *47*, 283-292.

(2) Hanahan, D.; Coussens, L. M. Accessories to the Crime: Functions of Cells Recruited to the Tumor microenvironment. *Cancer Cell*. **2012**, *21*, 309-322.

(3) Wang, Y.; Chu, Y.; Yue, B.; Ma, X.; Zhang, G.; Xiang, H.; Liu, Y.; Wang, T.; Wu, X.; Chen, B. Adipose-derived Mesenchymal Stem Cells Promote Osteosarcoma Proliferation and Metastasis by Activating the STAT3 Pathway. *Oncotarget.* **2017**, *8*, 23803-23816.

(4) Wozniak, S. E.; Gee, L. L.; Wachtel, M. S.; Frezza, E. E. Adipose Tissue: The New Endocrine Organ? A Review Article. *Dig. Dis. Sci.* **2009**, *54*,1847-1856.

(5) Bonuccelli, G.; Avnet, S.; Grisendi, G.; Salerno, M.; Granchi, D.; Dominici, M.; Kusuzaki, K.; Baldini, N. Role of Mesenchymal Stem Cells in Osteosarcoma and Metabolic Reprogramming of Tumor Cells. *Oncotarget.* **2014**, *5*, 7575-7588.

(6) Chu, Y.; Tang, H.; Guo, Y.; Guo, J.; Huang, B.; Fang, F.; Cai, J.; Wang, Z. Adipose-derived Mesenchymal Stem Cells Promote Cell Proliferation and Invasion of Epithelial Ovarian Cancer. *Exp. Cell Res.* **2015**, *337*, 16-27.

(7) Vettor, R.; Milan, G.; Franzin, C.; Sanna, M.; De Coppi, P.; Rizzuto, R.; Federspil, G. The Origin of Intermuscular Adipose Tissue and its Pathophysiological Implications. *Am. J. Physiol. Endocrinol. Metab.* **2009**, *297*, E987-998.

(8) Lastra, G.; Manrique, C. Perivascular Adipose Tissue, Inflammation and Insulin Resistance: Link to Vascular Dysfunction and Cardiovascular Disease. *Horm. Mol. Biol. Clin. Investig.* **2015**, *22*, 19-26.

(9) Martine, L. C.; Holzapfel, B. M.; McGovern, J. A.; Wagner, F.; Quent, V. M.; Hesami, P.; Wunner, F. M.; Vaquette, C.; De-Juan-Pardo, E. M.; Brown, T. D.; Nowlan, B.; Wu, D. J.; Hutmacher, C. O.; Moi, D.; Oussenko, T.; Piccinini, E.; Zandstra, P. W.; Mazzieri, R.; Lévesque, J. P.; Daltonn, P. D.; Taubenberger, A. V.; Hutmacher, D. W. Engineering a Humanized Bone Organ Model in Mice to Study Bone Metastases. *Nat. Protoc.* **2017**, *12*, 639-663.

(10) Carvalho, M. R.; Lima, D.; Reis, R. L.; Correlo, V. M.; Oliveira, J. M. Evaluating Biomaterial- and Microfluidic-based 3D Tumor Models. *Trends Biotechnol.* **2015**, *33*, 667-678.

(11) Rodrigues, T.; Kundu, B.; Silva-Correia, J.; Kundu, S. C.; Oliveira, J. M.; Reis, R. L.; Correlo, V. M. Emerging Tumor Spheroids Technologies for 3D *in vitro* Cancer Modeling. *Pharmacol. Ther.* **2018**, *184*, 201-211.

(12) Chen, J. W. E., Pedron, S., Harley, B. A. C. The Combined Influence of Hydrogel Stiffness and Matrix-bound Hyaluronic Acid Content on Glioblastoma Invasion. *Macromol. Biosci.* **2017**, *17*, 1700018.

(13) Riching, K. M.; Cox, B. L.; Salick, M. R.; Pehlke, C.; Riching, A. S.; Ponik, S. M.; Bass, B. R.; Crone, W. C.; Jiang, Y.; Weaver, A. M.; Eliceiri, K. W.; Keely, P. J. 3D Collagen Alignment Limits Protrusions to Enhance Breast Cancer Cell Persistence. *Biophys J.* **2014**,*107*, 2546-2558.

(14) Vetsch, J. R.; Paulsen, S. J.; Müller, R.; Hofmann, S. Effect of Fetal Bovine Serum on Mineralization in Silk Fibroin Scaffolds. *Acta Biomater.* **2015**, *13*, 277-285.

(15) Kim, J. Y.; Yang, B. E.; Ahn, J. H.; Park, S. O.; Shim, H. W. Comparable Efficacy of Silk Fibroin with the Collagen Membranes for Guided Bone Regeneration in Rat Calvarial Defects. *J. Adv. Prosthodont.* **201**4, *6*, 539–546.

(16) Dadwal, U.; Falank, C.; Fairfield, H.; Linehan, S.; Rosen, C. J.; Kaplan, D. L.; Sterling, J.; Reagan, M. R. Tissue-Engineered 3D Cancer-in-Bone Modeling: Silk and PUR Protocols. *Bonekey Rep*. **2016**, *5*, 842.

(17) Guzman, A.; Ziperstein, M. J.; Kaufman, L. J. The Effect of Fibrillar Matrix Architecture on Tumor Cell Invasion of Physically Challenging Environments. *Biomaterials*. **2014**, *35*, 6954-6963.

(18) Stellavato, A.; La Noce, M.; Corsuto, L.; Pirozzi, A. V. A.; De Rosa, M.; Papaccio, G.; Schiraldi, C.; Tirino, V. Hybrid Complexes of High and Low Molecular Weight Hyaluronans Highly Enhance HASCs Differentiation: Implication for Facial Bioremodelling. *Cell Physiol. Biochem.* **2017**, 44, 1078-1092.

(19) Desiderio, V.; De Francesco, F.; Schiraldi, C.; De Rosa, A.; La Gatta, A.; Paino, F.; d'Aquino, R.; Ferraro, G. A.; Tirino, V.; Papaccio, G. Human Ng^{2+} Adipose Stem Cells Loaded *in vivo* on A New Crosslinked Hyaluronic acid-Lys Scaffold Fabricate a Skeletal Muscle Tissue. *J. Cell Physiol.* **2013**, 228, 1762-1773.

(20) Kundu, B.; Schlimp, C. J.; Nürnberger, S.; Redl, H.; Kundu, S. C. Thromboelastometric and Platelet Responses to Silk Biomaterials. *Sci. Rep.* **2014**, *4*, 4945.

(21) Kundu, B.; Kundu, S. C. Silk Sericin/Polyacrylamide *in situ* Forming Hydrogels for Dermal Reconstruction. *Biomaterials*. **201**2, 33, 7456-7467.

(22) da Silva, L. P.; Cerqueira, M. T.; Sousa, R. A.; Reis, R. L.; Correlo, V. M.; Marques, A. P. Engineering Cell-Adhesive Gellan gum Spongy-like Hydrogels for Regenerative Medicine Purposes. *Acta Biomater*. **2014**, *10*, 4787-4797.

(23) Cerqueira, M. T.; Pirraco, R. P.; Santos, T. C.; Rodrigues, D. B.; Frias, A. M.; Martins, A. R.; Reis, R. L.; Marques, A. P. Human Adipose Stem Cells Cell Sheet Constructs Impact Epidermal Morphogenesis in Full-Thickness Excisional Wounds. *Biomacromolecules* **2013**, *14*, 3997–4008.

(24) Bhattacharjee, P.; Kundu, B.; Naskar, D; Kim, H. W.; Bhattacharya, D.; Maiti, T. K.; Kundu, S. C. Potential of Inherent RGD Containing Silk Fibroin-Poly (Є-caprolactone) Nanofibrous Matrix for Bone Tissue Engineering. *Cell Tissue Res.* **2016**, 363, 525-540.

(25) Wang, X.; Cho, K.-S.; Son, A. Ultrasonication as a Rapid and High Yield DNA Extraction Method for Bacterial Gene Quantification by NanoGene Assay. *Biotechnol. Bioprocess Eng.* **2015**, 20, 1133-1140.

(26) Harley, B. A.; Kim, H. D.; Zaman, M. H.; Yannas, I. V.; Lauffenburger, D. A.; Gibson, L. J. Microarchitecture of Three-dimensional Scaffolds Influences Cell Migration Behavior via Junction Interactions. *Biophys. J.* **2008**, *95*, 4013-4024.

(27) Livak, K. J.; Schmittgen, T. D. Analysis of Relative Gene Expression Data Using Real-Time Quantitative PCR and tThe 2-ΔΔCT Method. *Methods* **2001**, *25*, 402–408.

(28) Bramanti, E.; Catalano, D.; Forte, C.; Giovanneschi, M.; Masetti, M.; Veracini, C. A. Solid State (13)C NMR and FT-IR Spectroscopy of the Cocoon Silk of Two Common Spiders. *Spectrochim. Acta A Mol. Biomol. Spectrosc.* **2005**, *62*,105-111.

(29) Mohd Azam, N.; Amin, K. The Physical and Mechanical Properties of Gellan gum Films Incorporated Manuka Honey as Wound Dressing Materials. *Mater. Sci. Eng.* **2017,** *209*, 012027.

(30) Dominici, M.; Le Blanc, K.; Mueller, I.; Slaper-Cortenbach, I.; Marini, F.; Krause, D.; Deans, R.; Keating, A.; Prockop, D.; Horwitz, E. Minimal Criteria for Defining Multipotent Mesenchymal Stromal Cells. The International Society for Cellular Therapy Position Statement. *Cytotherapy* **2006**, *8*, 315–317.

(31) Denhardt, D. T.; Mistretta, D.; Chambers, A. F.; Krishna, S.; Porter, J. F.; Raghuram, S.; Rittling, S. R. Transcriptional Regulation of Osteopontin and the Metastatic Phenotype: Evidence for a Ras-activated Enhancer in the Human OPN Promoter. *Clin. Exp. Metastasis.* **2003**, *20*, 77–84.

(32) Velupillai, P.; Sung, C. K.; Tian, Y.; Dahl, J.; Carroll, J.; Bronson, R.; Benjamin, T. Polyoma Virus-Induced Osteosarcomas in Inbred Strains of Mice: Host Determinants of Metastasis. *PLoS Pathog.* **2010**, *6*, e1000733.

(33) Valabrega, G.; Fagioli, F.; Corso, S.; Madon, E.; Brach del Prever, A.; Biasin, E.; Linari, A.; Aglietta, M.; Giordano, S. ErbB2 and Bone sialoprotein as Markers for Metastatic Osteosarcoma Cells. *Br. J. Cancer* **2003**, *10*, 396-400.

(34) Agustina, H.; Asyifa, I.; Aziz, A.; Hernowo, B. S. The Role of Osteocalcin and Alkaline Phosphatase Immunohistochemistry in Osteosarcoma Diagnosis. *Patholog. Res. Int.* **2018**, 6346409.

(35) Sadikovic, B.; Thorner, P.; Chilton-Macneill, S.; Martin, J. W.; Cervigne, N. K.; Squire, J.; Zielenska, M. Expression Analysis of Genes Associated with Human Osteosarcoma Tumors Shows Correlation of RUNX2 Overexpression with Poor Response to Chemotherapy. *BMC Cancer.* **2010**, *10*, 202.

(36) Baker, A. E. G.; Tam, R. Y.; Shoichet, M. S. Independently Tuning the Biochemical and Mechanical Properties of 3D Hyaluronan-based Hydrogels with Oxime and Diels-alder Chemistry to Culture Breast Cancer Spheroids. *Biomacromolecules.* **2017**, 18, 4373-4384.

(37) Ochi, A.; Hossain, K. S.; Magoshi, J.; Nemoto, N. Rheology and Dynamic Light Scattering of Silk Fibroin Solution Extracted from the Middle Division of *Bombyx mori* Silkworm. *Biomacromolecules.* **2002**, *3*, 1187-1196.

(38) Flory, P. J. Thermodynamics of High Polymer Solutions. *J. Chem. Phys.* **1942**, *10*, 59–61.

(39) Coutinho, D. F.; Sant, S. V.; Shin, H.; Oliveira, J. T.; Gomes, M. E.; Neves, N. M.; Khademhosseini, A.; Reis, R. L. Modified Gellan gum Hydrogels with Tunable Physical and Mechanical Properties. *Biomaterials.* **2010**, *31*, 7494–7502.

(40) Peyton, S. R.; Putnam, A. J. Extracellular Matrix Rigidity Governs Smooth Muscle Cell Motility in a Biphasic Fashion. *J. Cell Physiol.* **2005**, *204*, 198–209.

(41) Gulsuner, H. U.; Gengec, N. A.; Kilinc, M.; Erbil, H. Y.; Tekinay, A. B. Osteoselection Supported by Phase Separated Polymer Blend Films. *J. Biomed. Mater. Res.Part A* **2015**, *103A*, 154–161.

(42) Palamà, I. E.; Arcadio, V.; D'Amone. S.; Biasiucci, M.; Gigli, G.; Cortese, B. Therapeutic PCL Scaffold for Reparation of Resected Osteosarcoma Defect. *Sci. Rep.* **2017**, *7*, 12672.

(43) Yoo, M. K.; Kweon, H. Y.; Lee, K. G.; Lee, H. C.; Cho, C. S. Preparation of Semi-Interpenetrating Polymer Networks Composed of Silk Fibroin and Poloxamer Macromere. *Int. J. Biol. Macromol.* **2004**, *34*, 263-270.

(44) Zheng, Y.; Wang, G.; Chen, R.; Hua, Y.; Cai, Z. Mesenchymal Stem Cells in the Osteosarcoma Microenvironment: Their Biological Properties, Influence on Tumor Growth, and Therapeutic Implications. *Stem Cell Res. Ther.* **2018**, 9, 22.

(45) Paino, F.; La Noce. M.; Di Nucci, D.; Nicoletti, G. F.; Salzillo, R.; De Rosa, A.; Ferraro, G. A.; Papaccio, G.; Desiderio, V.; Tirino, V. Human Adipose Stem Cell Differentiation is Highly Affected by Cancer Cells Both *in vitro* and *in vivo*: Implication for Autologous Fat Grafting. *Cell Death Dis.* **2017**, *8*, e2568.

(46) Dehouck, B.; Fenard, L.; Dehouck, M. P.; Pierce, A.; Tropier, G.; Cechelli, R. A New Function for the LDL Receptor: Transcytosis of LDL Across the Blood-brain Barrier. *J. Cell Biol.* **1997**, *138*, 877-889.

(47) De Francesco, F.; Tirino, V.; Desiderio, V.; Ferraro, G.; D'Andrea, F.; Giuliano, M.; Libondi, G.; Pirozzi, G.; De Rosa, A.; Papaccio, G. Human CD34/CD90 ASCs are Capable of Growing as Sphere Clusters, Producing High Levels of VEGF and Forming Capillaries. *PLoS One*. **2009**, *4*, e6537.

(48) Quent, V. M.; Loessner, D.; Friis, T.; Reichert, J. C.; Hutmacher, D. W. Discrepancies between Metabolic Activity and DNA Content as Tool to Assess Cell Proliferation in Cancer Research. *J. Cell Mol. Med.* **2010**, *14*, 1003-1013.

(49) Ashley, D. M.; Bol, S. J.; Waugh, C.; Kannourakis, G. A Novel Approach to the Measurement of Different *in vitro* Leukaemic Cell Growth Parameters: The Use of PKH GL Fluorescent Probes. *Leuk. Res.* **1993**, *17*, 873-882.

(50) Boutonnat, J.; Barbier, M.; Muirhead, K.; Mousseau, M.; Grunwald, D.; Ronot, X.; Seigneurin, D. Response of Chemosensitive and Chemoresistant Leukemic Cell lines to Drug Therapy: Simultaneous assessment of Proliferation, Apoptosis, and Necrosis. *Cytometry*. **2000**, 42, 50–60.

(51) Pathak, A.; Kumar, S. Independent Regulation of Tumor Cell Migration by Matrix Stiffness and Confinement. *Proc. Natl. Acad. Sci. U. S. A.* **2012**, *109*, 10334-10339.

Table 1: Primer sequences used for real-time PCR analysis of mRNA expression of target and housekeeping

Gene	Primer sequences	Amplicon (bp)	Annealing T (ºC)	ID
OPN	Rv - GGGGACAACTGGAGTGAAAA Fw - CCCACAGACCCTTCCAAGTA	244	56.2	NM 000582.2
BSP	Rv - CTTCCAACAGCCAATCACTG Fw - ACTGAGCCTGTGTCTTGAAA	102	59.4	NM 001330205.1
OCN	Rv- TCAGCCACTCGTCACAGC Fw - GTGCAGAGTCCAGCAAAGG	549	59	NM_020773.3
RUNX2	Rv - CAGCGTCAACACCATCATTC Fw - TTCCAGACCAGCAGCACTC	181	58.1	NM_001024630.4
GAPDH	Rv - GTCATGAGTCCTTCCACGAT Fw - AGCCTCAAGATCATCAGCAA	101	-	NM_001289745.2

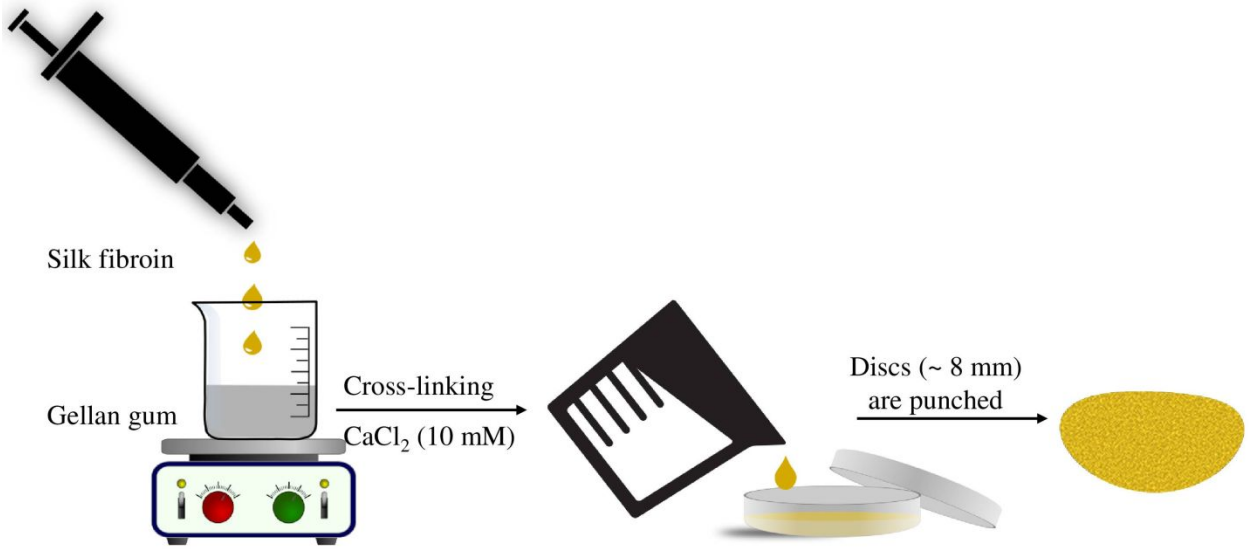

	Gellan gum-silk ratio	Gellan gum (vol%)	Silk (vol%)
G75: S25	3:1	75	25
G50: S50	1:1	50	50
G25: S75	1:3	25	75

Scheme 1: Schematics of gellan gum-silk fibroin spongy-like hydrogels preparation and summary of formulations.

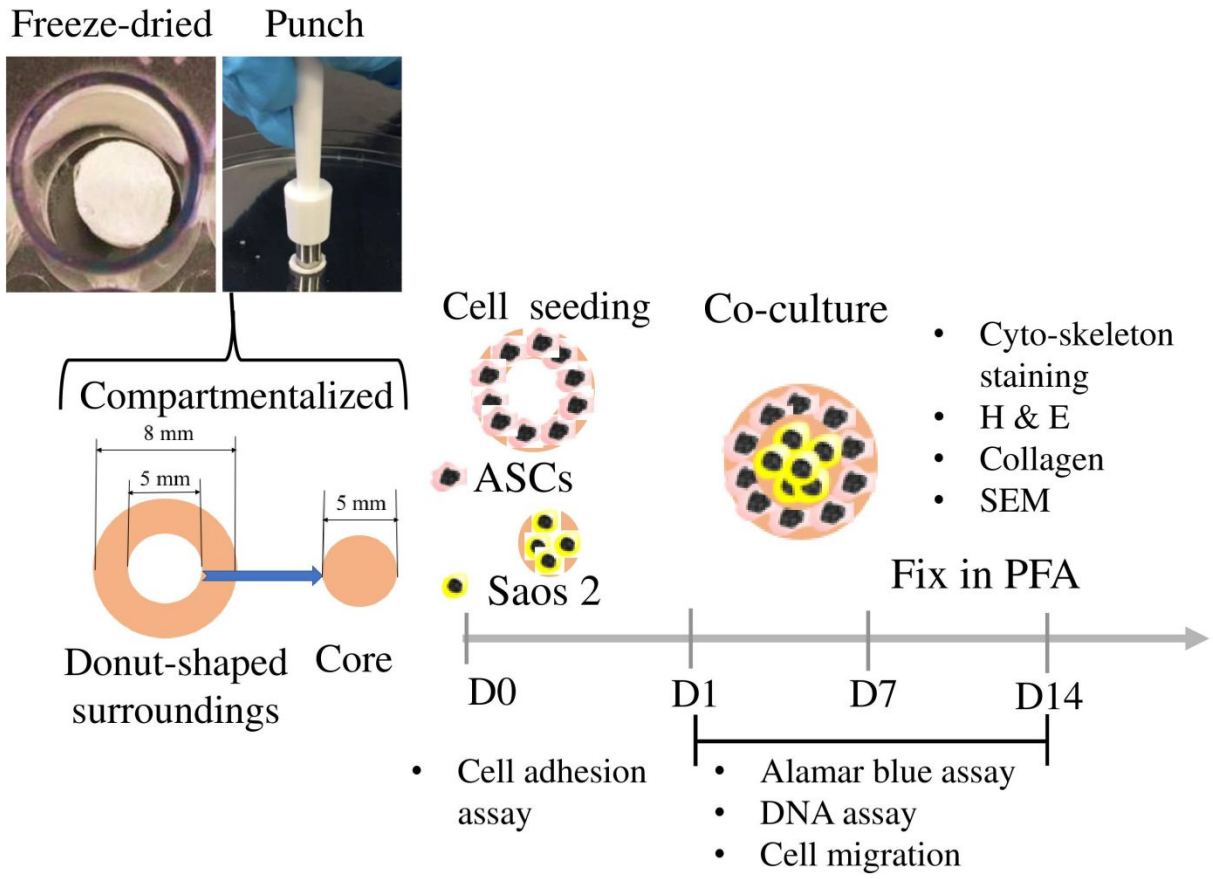

Scheme 2: Preparation of cell-laden gellan gum-silk fibroin 3D compartmentalized construct and experimental outline. Aqueous-based gellan gum-silk fibroin sponges (~ 8 mm diameter) are obtained by freeze-drying method. Discs around 5 mm diameter are cut out using biopsy puncher at the central space of 8 mm sponge; leaving behind a donut like shape. The center sponges are pre-seeded with human osteosarcoma cells (Saos 2); while donut-shaped sponges are seeded with human adipose derived stem cells (hASCs) and culture together to investigate the cross-talk between cells at different time-points.

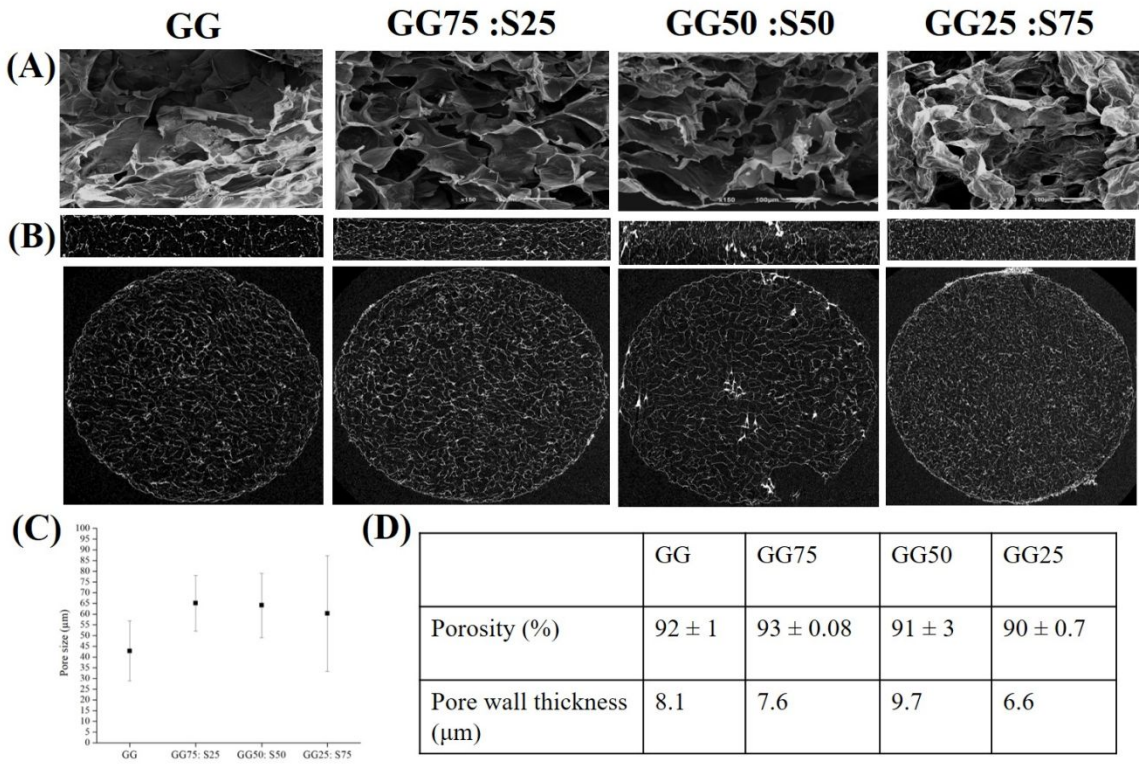

	GG	GG75	GG50	GG25
Porosity (%)	92 ± 1	93 ± 0.08	91 ± 3	90 ± 0.7
Pore wall thickness (µm)	8.1	7.6	9.7	6.6

Figure 1: (A) Scanning electron micrographs of freeze-dried hydrogels revealing pore structures and inter-connectivity. Scale bar is 100 µm. (B) Visualization of freeze-dried spongy-like hydrogels based on 3D images reconstructed using the DataViewer software revealing its microstructure in the transversal plane (below) and sagittal plane (up). (C) Pore size distribution of hydrogels with polymer blending ratios. (D) Table summarizing the porosity and pore wall thickness of spongy-like hydrogels in composition dependent manner, as obtained by microCT observation.

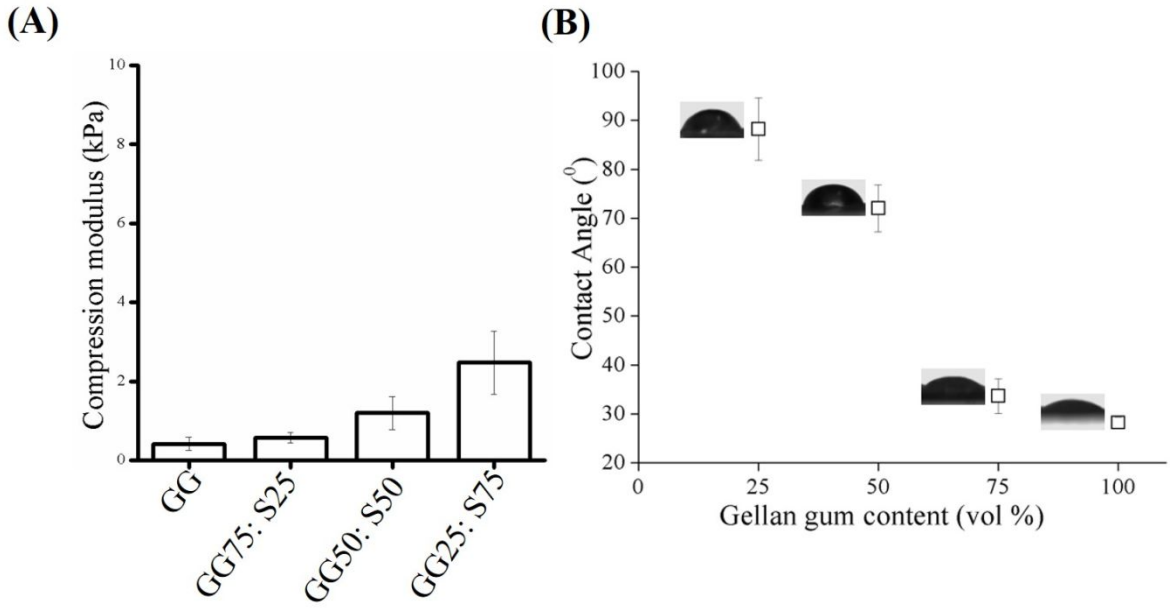

Figure 2: (A) Composition dependent compressive modulus (E_c) of hydrogels. (B) Wettability of freeze-dried hydrogels measured by means of contact angle using milli-Q water.

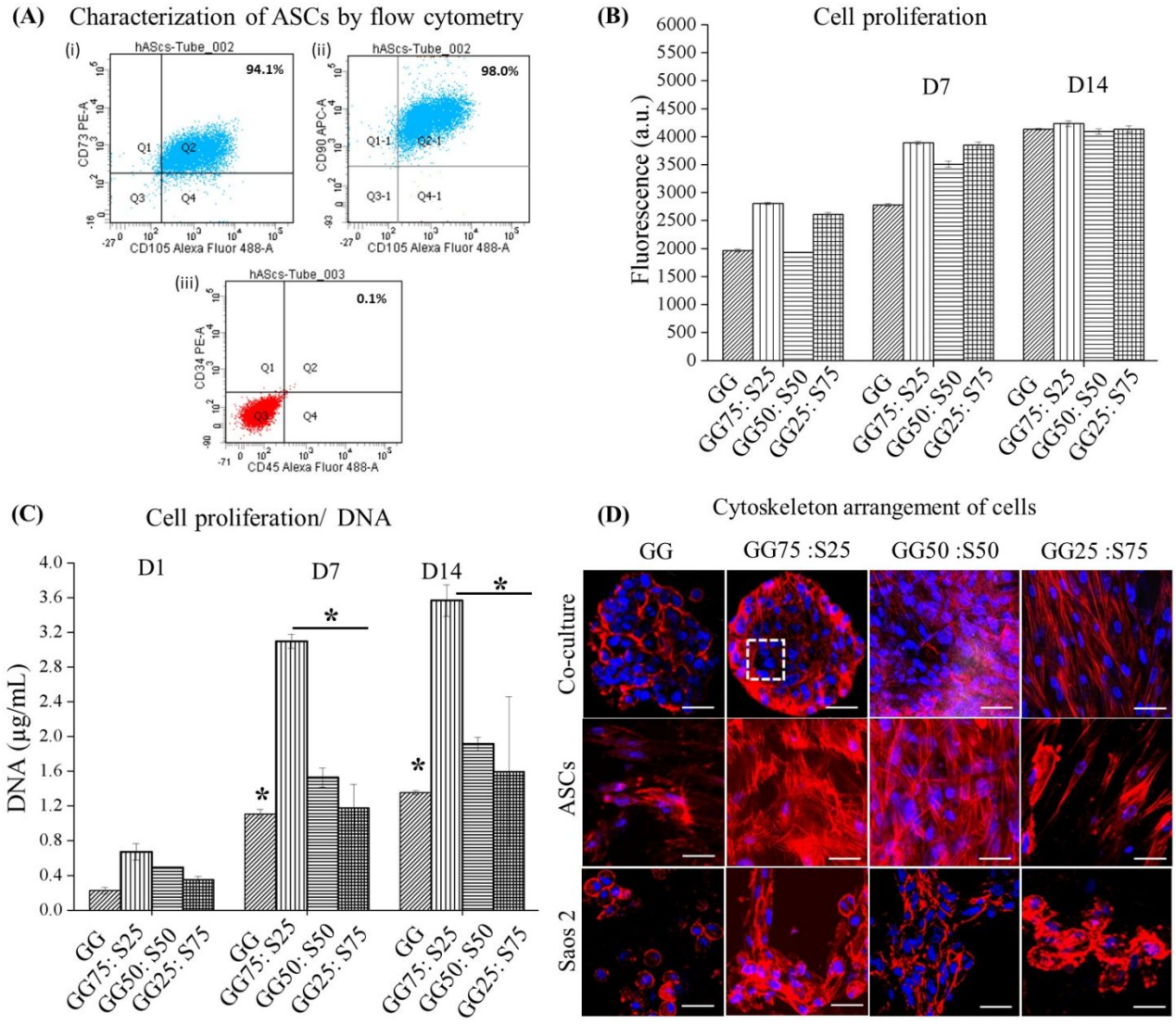

Figure 3: (A) Characterization of ASCs by flow cytometry; (B) Cell proliferation; and (C) DNA content of cells/construct (cells laden hydrogels) over time as assessed by Alamar Blue and PicoGreen assays, respectively. (D) Confocal laser scanning micrographs of rodhamine-labeled phalloidin stained actin of constructs (cell-laden compartmentalized hydrogel) and counterstained with DAPI after coculturing Saos 2 and adipose stem cells for 14 days. Scale bar = 50 µm.

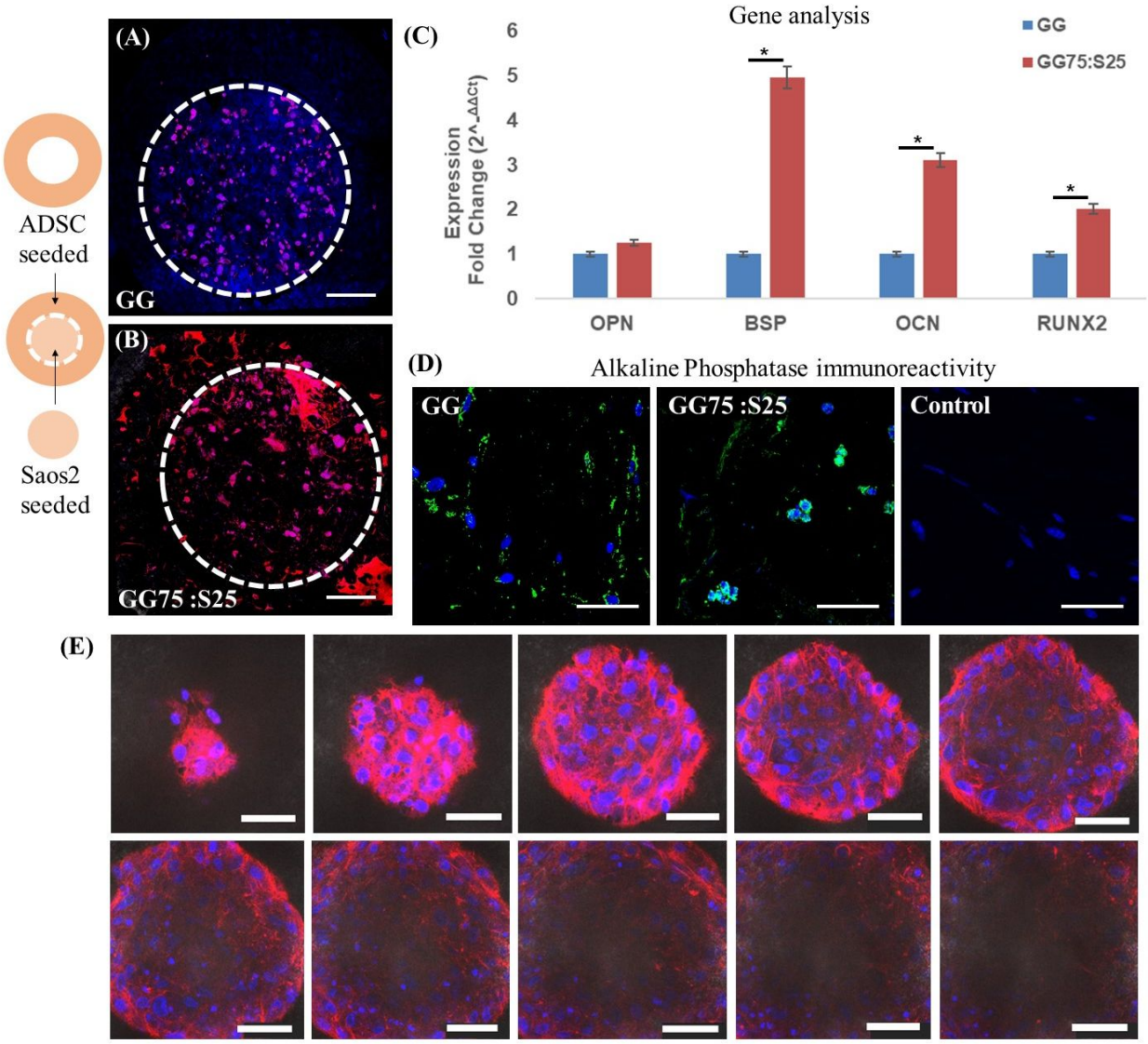

Figure 4: Confocal laser scanning micrographs reveal the distribution of cell spheroids at center of the compartmentalized hydrogel system, (A) GG and (B) GG 75: S25. Scale bar = 100 µm. ASCs are seeded into outer doughnut shaped hydrogel while Saos 2 are seeded in inner core as illustrated schematically. (C) Expression analysis of osteosarcoma-related genes. * p<0,01; (D) Fluorescence micrographs of immunoreactivity of alkaline phosphatase (green), counterstained with DAPI (blue) for nucleus. The section, which is only treated with fluorescence tagged secondary antibody in absence of primary ALP antibody and counterstained with DAPI (blue) for nucleus is served as controlled. Scale bar = 50 µm. (E) Z-Stacked images of Tumoroids obtained after co-culturing Saos 2 with ASCs in GG75: S25 for 14 days. Actins are stained with rodhamine-labeled phalloidin and nucleus are with DAPI. Scale bar = 50 µm.

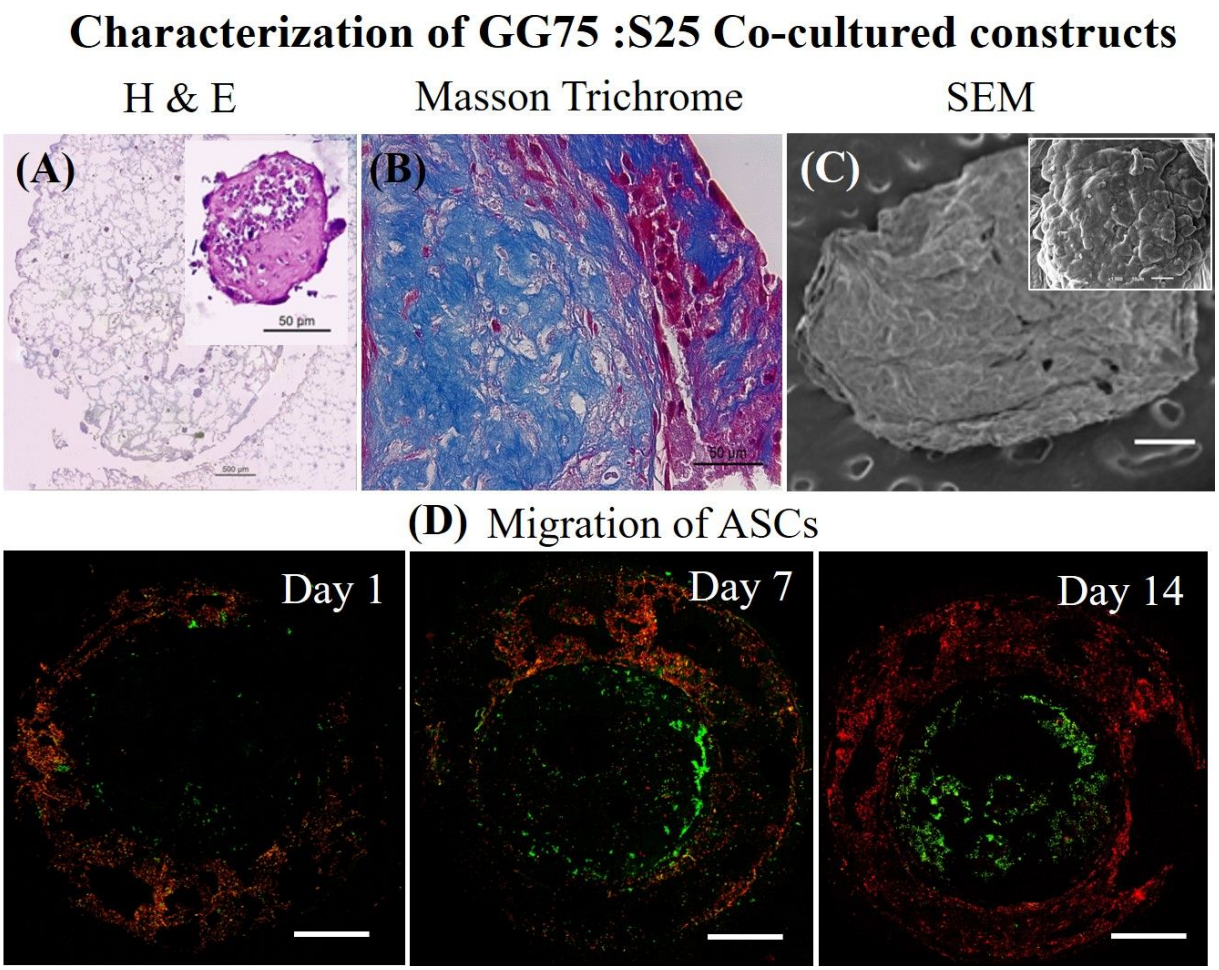

Figure 5: (A) Hematoxylin and eosin staining of GG75: S25 constructs and the detail morphology of the cell-aggregates (the inset pictures). (B) The detection of neo-collagen synthesized by GG75: S25 co-cultured construct. The biomarker is stained as blue. Scale bar = 50 μm. (C) The compartmentalized hydrogel system appeared as one entity in SEM image with a relatively smaller size, which is indicative of matrix degradation and remodeling. Scale bar = 500 μm. Inset individual co-cultured spheroids. (D) Time-dependent migration of ASCs towards Saos 2 over a period of 14 days. ASCs and Saos 2 are labelled separately with PKH26 Red Fluorescent Cell Linker and PKH67 Green Fluorescent Cell Linker, respectively for easy visualization. Scale bar = 100 μm.

Graphical abstract